Quantifying Pelagic Primary Production and Respiration via an Automated In-Situ Incubation System

By

Solomon T Chen

B.S. & B.A., University of Hawai‘i at Mānoa, 2020

Submitted to the Department of Earth, Atmospheric and Planetary Sciences
in partial fulfillment of the requirements for the degree of

Master of Science

at the

MASSACHUSETTS INSTITUTE OF TECHNOLOGY

and the

WOODS HOLE OCEANOGRAPHIC INSTITUTION

February 2023

Signature of Author 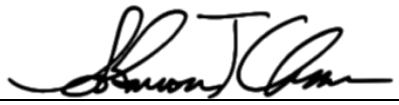

Joint Program in Oceanography/Applied Ocean Science and Engineering
Massachusetts Institute of Technology
And Woods Hole Oceanographic Institution
December 15, 2022

Certified by 

Dr. Matthew H. Long
Thesis Supervisor
Woods Hole Oceanographic Institution

Accepted by

Prof. Edward A. Boyle
Chair, Joint Committee for Chemical Oceanography
Massachusetts Institute of Technology
Woods Hole Oceanographic Institution

Quantifying Pelagic Primary Production and Respiration via an Automated In-Situ Incubation System

By

Solomon T Chen

Submitted to the Department of Earth, Atmospheric and Planetary Sciences
on December 15, 2022, in partial fulfillment of the requirements for the degree of

Master of Science

at the MASSACHUSETTS INSTITUTE OF TECHNOLOGY

and the WOODS HOLE OCEANOGRAPHIC INSTITUTION

Abstract

Pelagic photosynthesis and respiration serve critical roles in controlling the dissolved oxygen concentration (DO) in seawater. The consumption and production via pelagic primary production are of particular importance in surface ocean and in shallow aquatic ecosystems where photosynthetically active radiation (PAR) is abundant. However, the dynamic nature and large degree of heterogeneity in these ecosystems pose substantial challenges for providing accurate estimates of marine primary production and metabolic state. The resulting lack of data in these systems hinders efforts in scaling and including primary production in predictive models. To bridge the gap, we developed and validated a novel automated water incubator that measures in-situ rates of photosynthesis and respiration. The automated water incubation system uses commercially available optodes and microcontrollers to record continuous measurements of DO within a closed chamber at desired intervals. With fast response optodes, the incubation system produced measurements of photosynthesis and respiration with hourly resolution, resolving diel signals in the water column. The high temporal resolution of the timeseries also enabled the development of Monte-Carlo simulation as a new data analysis technique to calculate DO fluxes, with improved performance in noisy timeseries. Deployment of the incubator was conducted near Ucantena Island, Massachusetts, USA. The data captured diel fluctuations in metabolic fluxes with hourly resolution, allowed for a more accurate correlation between oxygen cycling and environmental conditions, and provided improved characterization of the pelagic metabolic state.

Thesis Supervisor: Dr. Matthew H. Long

Title: Associate Scientist

Woods Hole Oceanographic Institution

Acknowledgement

This thesis work was supported by NSF OTIC grant 1841092 to PI Collin Ward and Matt Long and WHOI Academic Office. The early work was also supported by NSF-REU Summer Student Fellowship program at WHOI. The subsequent development portion of this project was supported by WHOI-ADI OCIA to PI Matt Long and Ben Van Mooy.

I would like to thank my advisor Matt, for the unconditional support both in and outside of research. Matt has guided me much through both science and life. I can not express my eternal gratitude in words.

I would also like to extend my gratitude to all members of the MACHINE Lab. I would like to thank Dr. Jeff Coogan and Dr. Adam Subhas for all the advice and critical thinking, helping me zoom out and look at the big picture when needed.

For my mom Amy and my brothers Mathew and Feynman, we are who we are today because we have each other.

There are many people to thank during my journey at the MIT-WHOI joint program, and I would like to formally name each and every one of them in this paragraph. For my friends, firstly, I would like to acknowledge Antia, for being the one and only twin flame. Secondly, I would like to formally thank all the past and current members of 6 Cherry Street, I will smite any of you if I am not invited to your weddings. Moreover, I would like to thank my Seattle boys Josh and Henrik for always being there— we dragged each other off the Himalayas, and we will always have each other's back. Next, I would like to thank Ellen, for being an extraordinary friend and for introducing me to Brandon. As for Brandon, may sunset, Italian foods, and pretty girls be with you always, Amen. I also need to thank my favorite JP student Erica, for always being true, honest, and chill. Special shoutout to my favorite Chinese American, Shouyi Wang, you win sum you dim sum. Another special shoutout to my favorite half Asian sister, Olivia, for just being yourself and being here for me. Thank you to Olive for the wise words, "Ordinary is all there ever was". Thank you, Jonas, for the wise words, "Ocean only cools and alters rocks, my freezer does the same to my chicken". Finally, I would like to thank many of my fellow JP students for seeing me through my thick and thin, for supporting me, and for putting up with me.

Next, I would like to thank my 'Ohana back home in Hawai'i. Noah, Shaun, and Kealohi are basically my family and have treated me as such since my first day in GES. I also like to thank Dr. Michael Guidry for being an extraordinary mentor even after I have finished my GES degree.

I am but a humble surfer boy. I have learned much and would like to learn more. I love 'Āina and the people it nourishes, even though I can be impatient sometimes.

All glory goes to my family, forever and always.

Contents

List of Figures

Introduction

The increasing demand for pelagic primary production and respiration data has prompted recent methodological developments, aimed at providing a more accurate and cost-effective way to quantify metabolic processes (Ducklow and Doney, 2013; Collins et al. 2018; Long et al. 2019). Estimates of aerobic respiration and primary production in marine ecosystems are crucial for research and modeling efforts across a wide range of disciplines in marine and environmental sciences (del Giorgio and Williams, 2005; Staehr et al. 2012). For example, measurements of respiration and primary production determine the metabolic state of marine ecosystems (i.e., autotrophic or heterotrophic), help identify metabolic processes in the meso- and bathypelagic zone, and validate biogeochemical fluxes in global climate models (Reinthaler, et al, 2010; Duarte et al. 2013; Williams et al. 2013). The measurements of these two metabolic parameters can also provide crucial data for management practices such as wastewater treatment and coastal/estuarine restoration (Spanjers et al. 1994; Benway et al. 2016).

Despite the growing demand and importance of metabolic rate measurements, the development of reliable new methods has not kept pace (del Giorgio and Williams, 2005). Recent research has reported a large degree of uncertainty in metabolic measurements as traditional methods suffer from various biases such as bottle effects, mismatch of spatiotemporal scales, and the heterogeneity and complexity of the open ocean (Ducklow and Doney, 2013; G. Najjar et al. 2018). Most methods of measuring metabolic rates fall into two categories: (1) in-vitro incubation techniques track the rate of change in DO or dissolved inorganic carbon (DIC) in discrete water samples, while (2) in-situ techniques utilize geochemical tracers such as isotopic compositions of DO or DIC within water masses. Early measurements of pelagic respiration rates were often generated with in-vitro methods. This class of in-vitro incubation approach includes two-point

incubations utilizing Winkler titrations (Gaarder and Gran, 1927), ^{14}C-spiked incubations (Nielsen, 1952), or electron transfer activities (Kenner and Ahmed, 1975). In-vitro incubation methods are sensitive to short-term perturbations, such as diel variability, vertical plankton migration, upwelling, and weather events. Moreover, the two-point measurements provide flexibility to sampling procedures and experimental designs, especially for shipboard operations. These advantages have led to the continued dominance of in-vitro approaches in metabolic process measurements, with few methodological advancements over time.

By contrast, the application of in-situ methods has increased considerably due to advancements in instrumentation and sensing technologies. Recent technological advancements in optical sensors and mass spectrometry have enabled wider spatiotemporal coverage (Moore et al. 2009; Goldman et al. 2015). With continuous improvements in optical sensor technology and analysis techniques, low-power optical sensors and instruments are increasingly adapted by underwater autonomous vehicles and mooring platforms. The developments in in-situ geochemical tracer techniques and the integration of sensors are essential to long-term autonomous deployments and monitoring. However, the in-situ techniques also come with technical difficulties in resolving short-term perturbations inherent in the natural environment.

In-vitro and in-situ methods have respective advantages and faults, which have been debated for their unexplained discrepancy between the rates estimated by each method. For example, the in-situ O_2/Ar technique tends to yield positive net community production (NCP) while the in-vitro incubation techniques tend to indicate net heterotrophy at the same study site (Williams et al. 2004; Quay et al. 2010). The discrepancy can be organized into two categories of potential bias: (1) the time scale and processes targeted by the given methods and (2) the uncertainty inherent in the method chosen to quantify rates. Firstly, the in-vitro incubation approach tends to provide a

snapshot of the metabolic state of the ocean (e.g., the instance at which a water sample is taken) while the in-situ geochemical tracer approach focuses on steady-state and equilibrium on a longer timescale (e.g., integration of biological activity over days to weeks, depending on the residence time of tracer used). In this comparison, short-term natural perturbations of the water column can drastically alter in-vitro incubation results. Comparatively, the in-situ geochemical tracer methods tend to smooth out short-term variability by assuming steady state of the tracer budget (e.g., O_2, ^{13}C). However, the in-situ approach requires integrating across the water column, where complex and unresolved physical transport processes such as vertical mixing, lateral advective, and air-sea gas exchange increase uncertainty in the resulting rates (Williams et al. 2013). The depth of integration can also bias, attenuate, or result in a lack of resolution in rate estimates (e.g., mixed layer depth, photic depth) (Palevsky & Doney, 2018). Both in-vitro and in-situ methods also lack sufficient temporal resolution to describe diel cycling of metabolic processes. The in-situ method can only resolve equilibrium on the longer timescale (e.g., weeks), while in-vitro incubations often determine metabolic rates with two-point measurements (i.e., beginning and end of incubations, often on the scale of days).

In addition to bias in timescales and the targeted processes, the inherent uncertainty in chosen analytical methods also contributes to overall bias. For example, the in-situ O_2/Ar method via mass spectrometry is estimated to have 0.05% uncertainty for the O_2/Ar ratio, better than the ~1% uncertainty in O_2 concentrations produced by Winkler titrations (Hamme and Emerson, 2006). In-vitro incubations have also been plagued by contamination and disruption during sampling and preparation processes, biasing the results by hindering metabolic processes or changing the microbial community structure in unexpected ways (Suter et al. 2017). The discrete sampling of in-vitro methods also suffers from “bottle effects”, where unsystematic errors and heterogeneity

in the ocean are amplified by sampling and analyses procedures. In-vitro incubations also often suffer from unrepresentative incubation conditions where laboratory incubations fail to reproduce the complex variation in the natural environment such as temperature, pressure, and light level fluctuations. Failing to emulate key environmental conditions affects processes dependent on those conditions (i.e., photosynthesis is primarily driven by light, and respiration rates are tightly linked to temperature, pressure, and availability of nutrients).

Recently, technological advances in sensors and engineering controls have led to the development of automated water incubators that can be constructed at lower costs while having higher sampling frequencies. This new class of in-situ instrumentation has sought to build upon and integrate the most advantageous components of previous in-vitro and in-situ methods. Pioneering examples include benthic flux chambers and recent developments of small bottle incubators (Lee et al. 2015; Collins et al. 2018; Long et al. 2019). These incubators combine commercially available sensors and embedded microcontrollers to automate measurements. The increased temporal resolution of data collected from fast response sensors also enables more rigorous statistical analyses that increase metabolic rate accuracy.

Here, we describe an automated light and dark chamber incubation system for measurements of respiration and primary production with a high temporal resolution. Our automated incubator system can resolve hourly metabolic fluxes in a self-contained unit. The automated incubation system minimizes the impacts of biofouling using ultraviolet (UV) LEDs and UV transparent materials. Data analysis using Monte-Carlo simulation techniques to determine high-frequency and robust estimation of metabolic rates. Finally, we provide recommendations for incubation lengths based on the targeted metabolic rates and signal-to-noise ratio of the sensor used. Overall, this new class of automated, in-situ incubation systems is expected to be highly useful in

determining high-resolution pelagic metabolic rates that can be implemented on a range of ocean moorings, vehicles, and floats to provide vital rates for global ocean modeling.

Method and Materials

Study site

The incubation system was deployed on the south shore of Uncatena Island, a small island located on the southern end of Cape Cod in Massachusetts, U.S.A. (Figure 1). The instrument was attached to an anchor ~70 m offshore from a sandy beach at ~1.5 m deep (41° 31'3" N, 70° 42'3" W) over 4 test deployments between August and October 2021. The benthic surface at the deployment site was dominated by seagrass (*Zostera marina)*, underlaid by mixed gravel, and mud sediments.

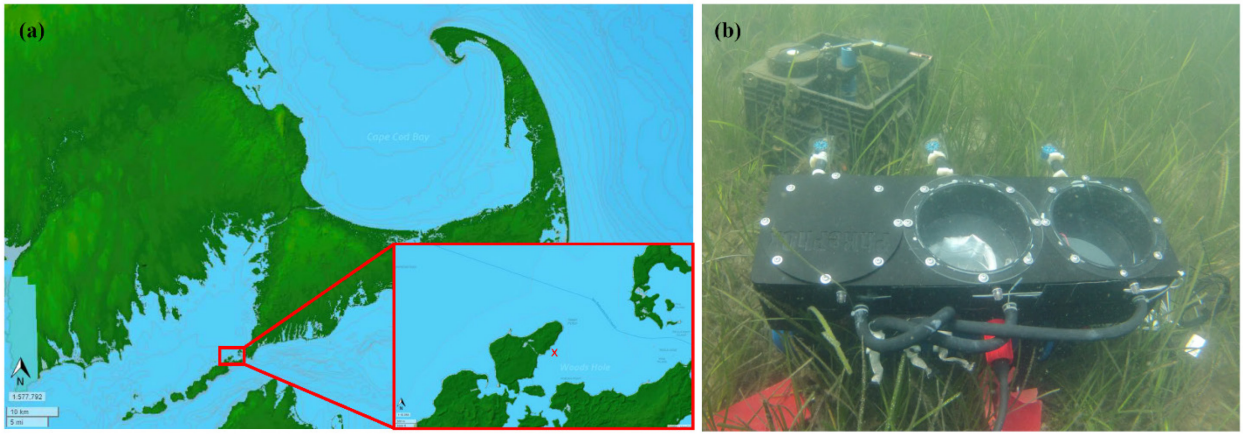

Figure 1. (a) A map showing the location of deployment site at the southern end of Cape Cod (MassGIS), (b) and the automated incubator displayed at deployment site near Ucantena Island.

Automated Incubation System

An automated incubation system was developed to conduct hourly incubations and produce oxygen consumption/production rates. This design improved upon recently developed systems for both open ocean mooring and shallow coastal applications (Collins et al. 2018; Long et al. 2019).

The automated incubation system consisted of three incubation chambers, all capable of producing incubation measurements independently (Figure 1b). The main body of the system was machined out of Delrin plastic, hosting incubation chambers, pumps, and UV LEDs. The top half of the main body was three 1-liter cylindrical chambers for seawater incubations. The top side of the incubation chambers were enclosed by clear UV-transparent plastic (Arkema Oroglas UVT), quartz, or black Delrin plates to produce light and dark chambers, respectively. A low-pressure check valve was mounted near the highest level of each chamber for flushing, while another check valve acted as the chamber inlet and was located at the base of the incubation chamber. A sampling port for manual seawater extraction enabled water sampling for additional lab analyses. The bottom of each chamber was enclosed with a UV-transparent quartz plate to enable biofouling control within the chambers (see below). A PyroScience OXROB3 optode was inserted along with a thermistor to monitor DO concentration and temperature in each chamber. The bottom half of the main body was housing for UV LEDs, heatsinks, and pumps. Each chamber had a dedicated EWP-DC30A1230 pump (1.6 L $minute^{-1}$) with a 500 μm stainless steel mesh inlet filter. For UV irradiation, an IRTRONIX CA3535 chip was used for each chamber, which hosted a four-by-four array of 275 nm UV-C LEDs with 290 mW of radiant power output per array. The UV LED chips were mounted in the center of their housing at a distance of 5cm from the chamber to ensure the viewing angle of the LED chip overlapped with the quartz window on the bottom of each incubation chamber. The mounting position ensured that all surfaces of the chamber is irradiated during the biofouling control process. An external LED chip was mounted in a waterproof housing to irradiate the outside of the acrylic top plate, to prevent external biofouling that could reduce light transmission into the chamber (or a quartz top plate was used). A separate pressure housing contained a microcontroller (Teensy 3.6), electronic control units, PyroScience DO measurement

modules, analog-digital converters (ADC), and batteries (Figure 2). All UV LEDs and pumps were controlled by latching relays. Each LED chip was powered by a 500-mA constant current driver (Recom Power RCD24-0.50). Each PyroScience module was connected to a 16-bit Adafruit ADC board (ADS1115) for differential analog to digital conversion (ADC).

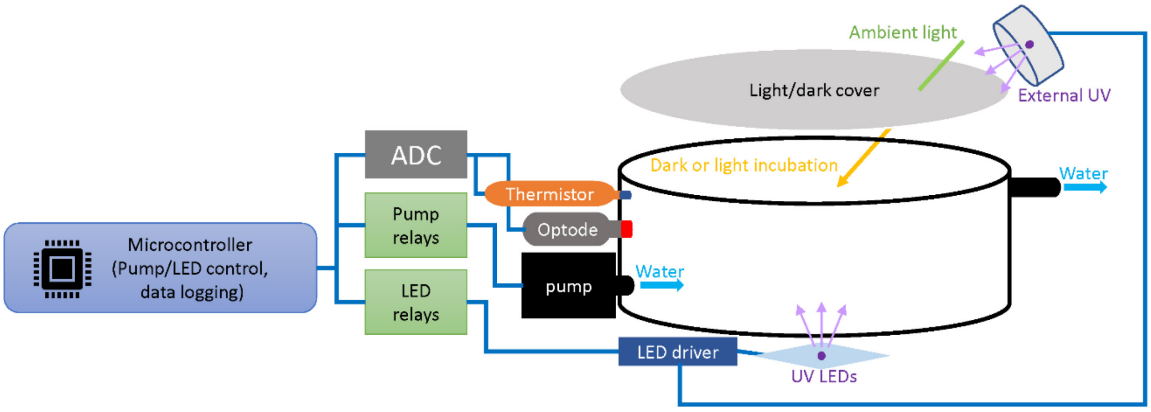

Figure 2. Schematic showing system architecture and wiring of the automated incubation system. The automated incubation system is in triplicate of this conceptual diagram. The Teensy 3.6 serves as the microcontroller and data logger. An internal and external LED, PyroScience sensor module, pump, relays, ADC, and LED power conditioning unit (drivers) are shown in this diagram. The complete instrument contained triplicates of each chamber and associated components.

In this study, the incubation system was programmed to conduct one-hour incubations. At the beginning of each hour, the sampling pump was triggered for a 5-min flushing period, flushing each chamber ~7 times (e.g., 0:00 to 0:05 minutes). After flushing, individual incubation chambers were sealed by the check valves for 50 minutes (e.g., 0:05 to 0:55 minutes), during which the integral optode and thermistor monitored DO concentrations continuously. At the end of the incubation period (e.g., minute 0:55), the UV LEDs were activated to irradiate the chamber for 5 minutes (e.g., 0:55 to 0:00) to minimize biofouling.

UV Biofouling Control

Biofouling occurs on all oceanographic instrumentation, often affecting the precision and accuracy of measurements that are exacerbated by extended deployment times (Ward, 2021). For measurements of pelagic productivity, the incubation system requires biofouling control to ensure the measurements do not exhibit a baseline shift in magnitude due to enhanced growth on surfaces or reductions in natural light supplied to each chamber. To assess the effectiveness of UV LED as biofouling control, experiments were designed based on a recent study reporting that biofilm growth on plastic films in the ocean was strongly linked to reductions in light transmittance (Nelson et al. 2021). The incubation system was submerged in a freshwater tank, supplemented with a natural microbial community. The incubation system was programmed to function as a normal field deployment. The UV LEDs irradiated each chamber hourly for different periods of time before the pumps flushed and renewed water samples within each incubation chamber. Triplicate low-density polyethylene (LDPE) films were placed in chambers programmed with different UV dosages for 27 days. Biofouling on the LDPE films was subsequently measured using the light transmission port of a UV-visible spectrophotometer (PerkinElmer Lambda 650s; Nelson et al. 2021). The UV dosages were varied by controlling irradiation time: 0, 5, and 10 minutes per hour-long incubation. The UV dosage is calculated from the UV irradiation level measured by a spectral radiometer (StellarNet Solar-Rad). In addition to UV treatments, LDPE samples were placed in a saturated mercury chloride solution as an abiotic control.

Metabolic Rate Calculation with Monte-Carlo Simulation

The automated incubation system offered improved temporal resolutions within each incubation period with ~1Hz sampling frequency compared to traditional methods, providing more statistical context for understanding metabolic processes. In this study, Monte-Carlo simulation was utilized

to extract the predominant oxygen consumption/production rates from the DO concentration data. For rate extraction via the Monte-Carlo simulation, a sample set of two DO concentrations was randomly sampled within the defined incubation time series, and the slope (R_s) between the given two points was calculated by equation 1:

$$R_s = \frac{[O_2]_f - [O_2]_i}{t_f - t_i} \qquad \text{Equation 1.}$$

where R_s is the calculated slope for the given sample set, $[O_2]$ is the DO concentration and t represents the elapsed timestamp for each point in the random sample set. The f subscript marks the endpoint while the i subscript marks the beginning point (earlier time) of the sample set. The technique then repeated random sampling and slope calculations over 2000 designated repetitions. Histograms were generated from all 2000 R_s values for each incubation period. All R_s were then binned by predefined binning resolutions (i.e., 500 bins for 2000 repetitions of R_s in this study). The mean value of peak bins with a combined weight of over 80% sample size was then calculated as the representative oxygen production/consumption rate (R_c) of the given incubation period by Equation 2:

$$R_c = \sum \frac{R_{set}}{n}$$

$$R_{set} = \{R_i \in all\ R_s \big| E_{low} < R_i < E_{high}\},\ n = |R_{set}| > repetition \times 80\% \qquad \text{Equation 2.}$$

where E_{high} and E_{low} are the higher and lower boundary of R_{set} selected for R_c calculation. In addition to calculating R_c, this study also investigated the optimal incubation length with the Monte-Carlo simulation technique. The goal was to quantify the shortest possible incubation length given the expected DO flux and signal-to-noise ratio (SNR) of the sensor used. The shortest possible incubation length was calculated by applying Monte-Carlo simulation on an artificially

generated dataset (A) with a given rate of change (a) and SNR (i.e., a straight line with a known slope and randomly generated noise according to a given SNR from the sensor used). The Monte-Carlo simulation was applied on increasing portions of the dataset until the simulation results correctly predicted the rate of change (i.e., the model repeated the simulation with increasing lengths of the dataset until the 5% error criteria was achieved). The shortest incubation length required ($t_{optimal}$) was then calculated based on the sampling frequency of sensor used (Equation 3).

$$t_{optimal} = |A| \times sampling\ frequency, A = \{y\ |y(x) = ax + SNR\} \quad \text{Equation 3.}$$

Results

Efficiency of UV Biofouling Control

The 27-day testing of different UV treatments (0, 5, or 10 minutes per hour) yielded substantial differences in biofouling, as inferred through the decrease of light transmission through the plastic films. The total UV dose (kJ) at the top of the incubator was calculated by multiplying the radiant power output by exposure time; the 5-minute UV irradiation (~5W m^{-1}) was equivalent to ~15 kJ, and the 10-minute UV irradiation was equivalent to 30 kJ. The extent of biofouling in each treatment was quantified at two major chlorophyll absorption peaks, 430-450 nm, and 665-685 nm (Figure 3a).

In the 430-450 nm region, the integrated transmittance exhibited significant differences between the UV-treated samples and the non-UV-treated samples (Figure 3b). On the third day of this timeseries, the transmittance of non-UV-treated samples decreased to ~84% while the transmittance of UV-treated samples stayed at ~88% for the first week of the trial. A general trend of decreasing transmittance was observed in the second half of the 27-day trial. On day 4, control,

UV treated, and non-treated showed significant differences (p-value < 0.05), while the UV-treated groups (5 and 10 minute irradiation) did not show significant differences via ANOVA test. The UV-treated groups showed efficacy for controlling biofouling until after day 24. On day 27, the 5-minute UV irradiation treatment group was not significantly different from the non-treated group.

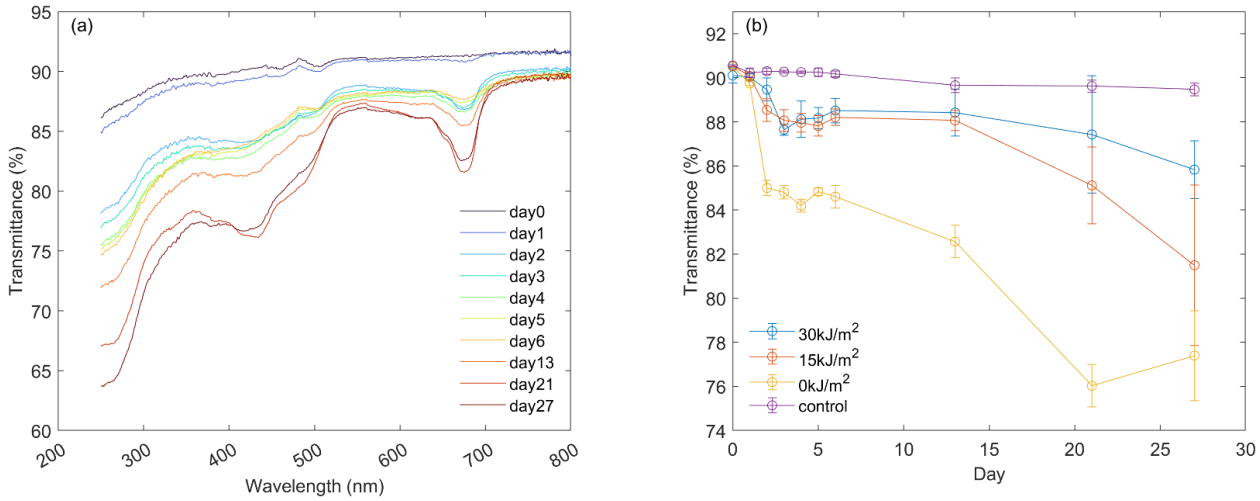

Figure 3. (a) Example spectra compilation from non-UV treated samples showing the evolution of transmittance spectra over time. Each line represents a transmittance spectrum at a given time point when LDPE films were retrieved and measured. (b) Integrated transmittance (%) for 430-450 nm wavelengths. The four treatment groups ranged from no UV exposure (yellow) to a dosage of 30 kJ m^{-2} at the end of each incubation cycle (blue).

Stability of Monte-Carlo Technique

The Monte-Carlo simulation technique relied on randomized sampling to generate histograms of the estimated rates for each incubation— each simulation may generate slightly different estimations as a result of randomized sampling (Figure 4). It is important to ensure the stability of the simulation outcome by using appropriate simulation parameters. Simulation parameter testing was conducted on a set of artificially generated samples with known statistical properties such as linear slope (R_s = 1) and noise-to-signal ratio (± 20% noise). The Monte-Carlo technique was applied with various parameters (e.g., number of repetitions, the width of bins, mean value

averaging criteria). The mean rate simulation results indicated the general simulation outcome reached stability as soon as the number of repetitions exceeded 2000, stability was indicated by the mean rate prediction (Figure 5a) and error of simulation outcome. The error of the simulation outcome was suppressed by increasing the number of repetitions, declining to lower than 2% uncertainty once the number of repetitions exceeded 4000 (Figure 5b). This test conceptually supported the use of the Monte-Carlo simulation technique in this application, since the noise magnitude from the optodes was much lower than the artificial dataset, and each incubation period provides an ample number of data points (~3000) for randomized sampling.

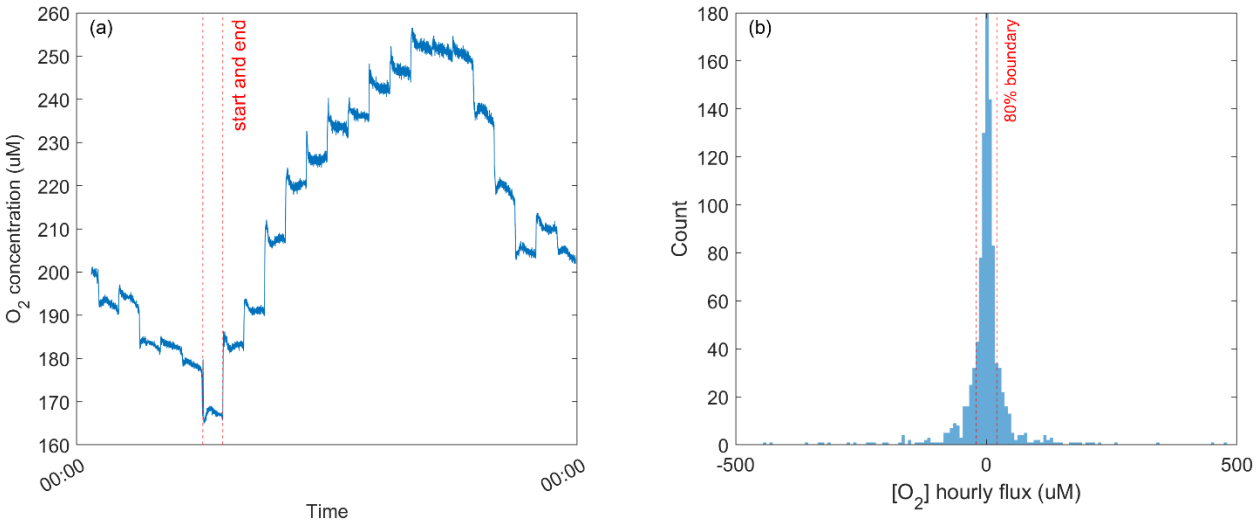

Figure 4. 4a shows an example DO time series from test deployment (8/26/2021). The rapid DO concentration shift indicates flushing of the incubation chamber at the end of each incubation period. The red dash lines represent the duration of one incubation period. 4b shows an example outcome histogram of Monte-Carlo simulation on a selected incubation period. The mean value within the 80% weight boundary is extracted as the DO consumption/production rate.

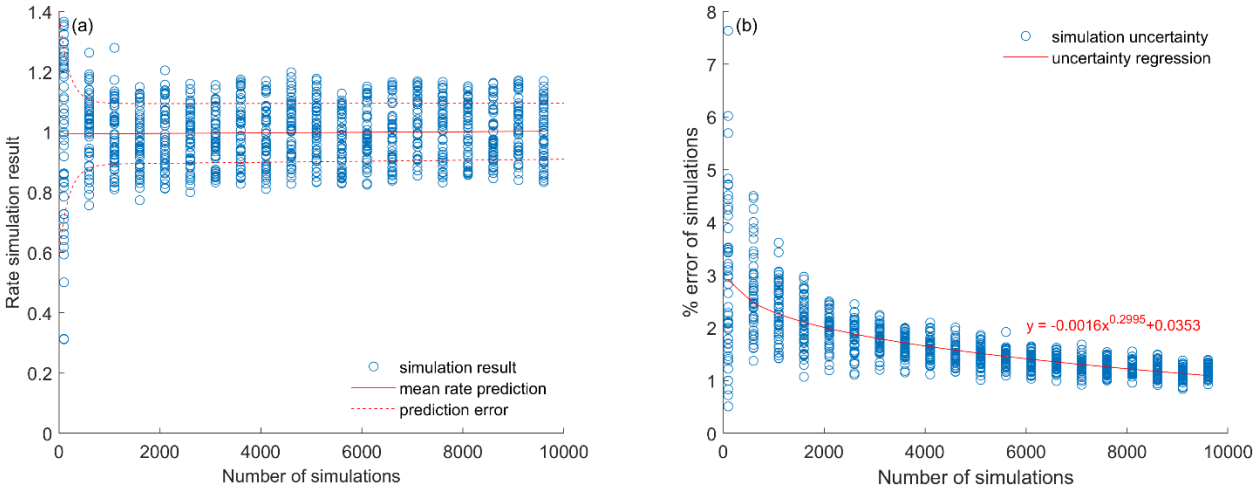

Figure 5. 5a illustrates the stability of Monte-Carlo simulation techniques with an increasing number of repetitions. The given dataset has a known slope (S = 1). The red line in 5a represents a linearly fitted line and the dash lines represent 1 standard deviation of prediction groups, suggesting the mean simulation results are effective at producing correct results even with added noise. 5b shows the decay of error in simulation as the number of repetitions increases. The % error of estimations is suppressed to below 2% after ~4000 repetitions.

Field Deployments and Data Products

The automated incubator was deployed for approximately 72 hours four times throughout the summer of 2021. The incubator was programmed to generate DO measurements at ~1Hz; each incubation period consisted of roughly 3000 measurements of DO concentration. The Monte-Carlo simulation was then applied to the time series of each incubation period respectively, generating a DO consumption/production rate (μMole L^{-1} hr^{-1}) for each hourly incubation. Field data shows hourly DO production rates from the light chamber and the DO consumption rate from the dark chamber (Figure 6).

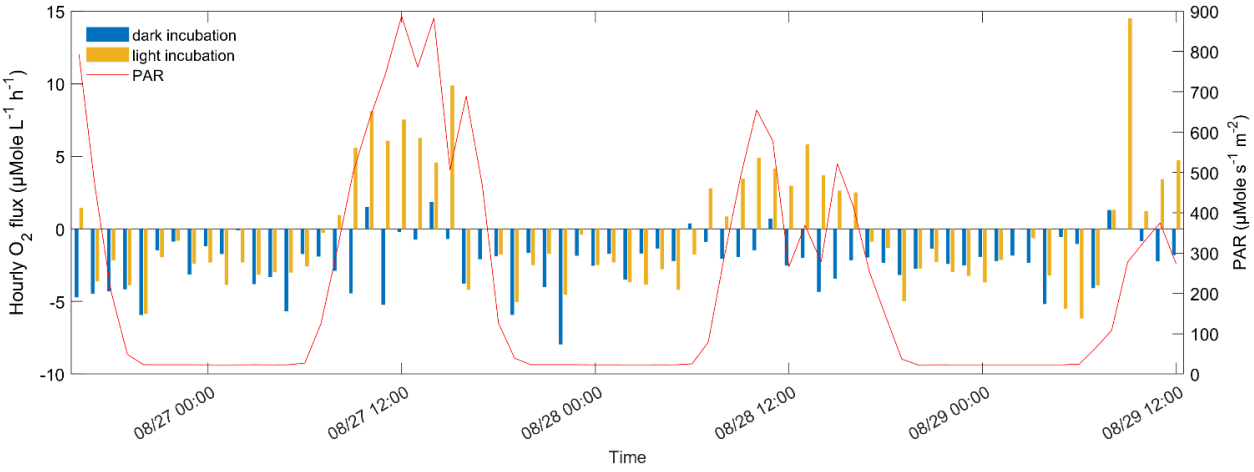

Figure 6. An example of field data at Ucantena Island on 8/26/2021-8/29/2021. The hourly O_2 fluxes are calculated for light (yellow bars) and dark chambers (blue bars). The red line represents hourly integrated PAR measurements. Data suggests that the automated incubation system is sensitive to short-term environmental conditions (e.g., diel cycles, PAR fluctuations).

The automated incubator was deployed for approximately 72 hours four times throughout the summer of 2021. The incubator was programmed to generate DO measurements at ~1Hz; each incubation period consisted of roughly 3000 measurements of DO concentration. The Monte-Carlo simulation was then applied to the time series of each incubation period respectively, generating a DO consumption/production rate (µMole L^{-1} hr^{-1}) for each hourly incubation. Field data shows hourly DO production rates from the light chamber and the DO consumption rate from the dark chamber (Figure 6).

With hourly O_2 fluxes calculated, more in-depth analyses were conducted to resolve the magnitude of photosynthesis and respiration. In respiration analysis, the goals were to determine 1) the mean respiration rate and 2) the required incubation length to achieve stable DO flux estimates. Instead of applying Monte-Carlo simulation to the full-length of DO timeseries in experiments, this analysis estimated rates with only part of the incubation length. Here, the Monte-Carlo simulation was applied to the first 5 minutes of the time series in each dark incubation experiment (n = 73), and then 10 minutes, and so on until the full length of the incubation experiment is reached (Figure

7a). A mean hourly respiration rate was calculated to be -1.62±1.17 μmol L^{-1} hr^{-1} O_2 at the deployment site.

For photosynthesis rate estimation, a trend between photosynthetically available radiation (PAR) and the oxygen production rate in the light chamber was observed in Figure 6. The oxygen production rate showed sensitivity to short-term fluctuation in hourly averaged PAR (Figure 7b). The relationship between PAR and photosynthetic DO fluxes can be characterized by comparing all in-situ hourly DO fluxes from the light chamber and the hourly integrated PAR measurements. In this analysis, DO flux from gross primary production (GPP) during the daytime (i.e., when underwater PAR measurements are non-zero) was calculated by adding the previously calculated mean respiration to net primary production (NPP) (Figure 7b). A logarithmic curve was fitted to indicate the general correlation between PAR and photosynthesis. The fitted curve indicated a light compensation point of 82.2 μMole s^{-1} m^{-2} and decreasing photosynthetic efficiency as PAR increased. However, light saturation was not apparent and GPP continued to increase across all measured light levels. Further, the DO flux rate could be compiled into an averaged diel DO flux estimate (Figure 8). The diel DO flux roughly follows the trend of averaged PAR and suggested that hourly photosynthetic fluxes were higher in the morning when compared to those in the afternoon with similar PAR levels (also see Figure 7b). Notably, the DO fluxes during dawn and dusk hours had higher uncertainties, reflecting the variability of DO flux directions during crepuscular periods. Finally, the daily net ecosystem metabolism (NEM) was calculated directly from the summation of the DO fluxes over 24hrs (Eq. 4) and then the GPP was calculated by equation 5:

$$NEM = \sum_{24}(hourly\ DO\ flux) \qquad \text{Equation 4.}$$

$$Hourly\ DO\ flux = NPP = GPP - R \qquad \text{Equation 5.}$$

The NEM at the deployment site was 2.56 ± 10.02 μmol O_2 L^{-1} d^{-1}, and the GPP was 49.59 ± 15.26 μmol O_2 L^{-1} d^{-1}. These estimates indicated that the water column was near the metabolic balance, driven by the high photosynthesis during the day. We observed no apparent seasonal trend across 4 deployments. Mean respiration rates and photosynthesis-PAR relationship were comparatively stable between late August and early October as the daily temperature range in the water was stable roughly between 24-29 ºC.

S

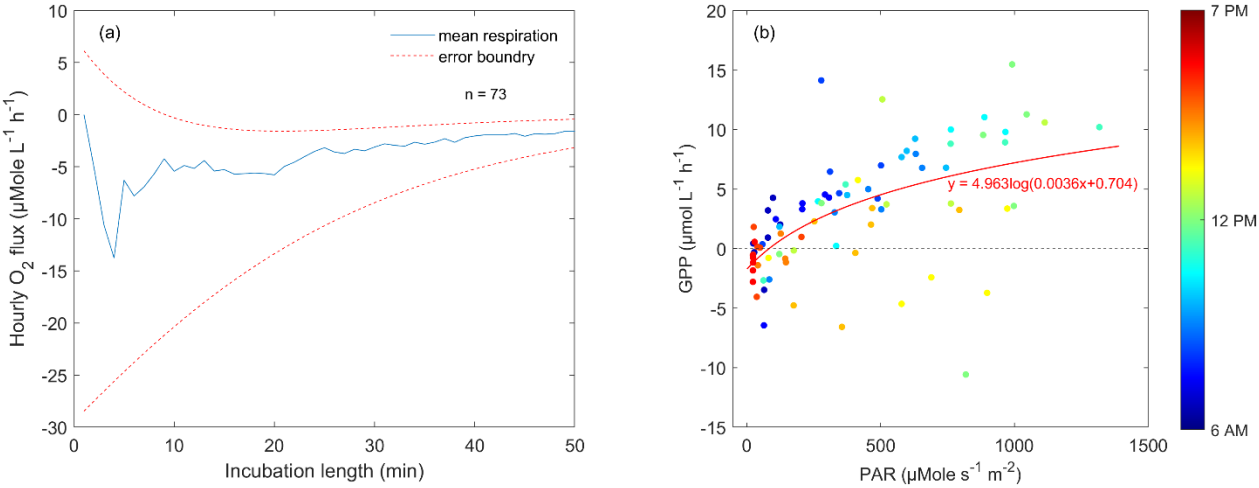

Figure 7. 7a shows respiration rates with different time constraints. The error boundary represents the furthest deviation of Monte-Carlo simulation results at the given time limit. 7b shows the correlation between photosynthetic rates in μMole L^{-1} h^{-1} O_2 and PAR from all test deployments.

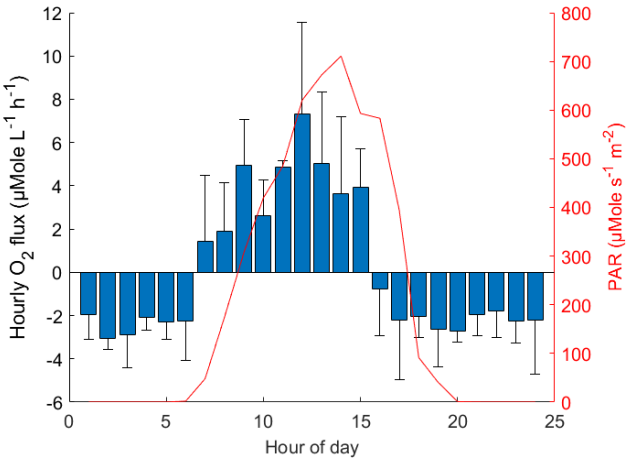

Figure 8. Averaged diel DO fluxes compiled from all field deployments. The diel signal was a result of the averaging of 4 testing deployments, each deployment spans ~72 hours. The error bar

indicates the standard deviations of the respective hourly DO fluxes. The red line is the hourly average PAR over all test deployment dates.

Optimal Incubation length

The optimal incubation length can be estimated by Monte-Carlo simulation using artificially generated timeseries (sampling frequency of 1 Hz), the sensor SNR, and the expected rate of change (e.g., O_2 flux) (Figure 9). The SNR and incubation length exhibited a relationship of exponential decay while the incubation length and expected O_2 flux share a polynomial correlation. The relationships between all three variables can be summarized in Equation 6:

$$t_{optimal} = 16.3 + 3.46 \times 10^{-4} SNR^2 \times R_c + 0.0713 \times SNR \times R_c - 0.332R_c$$

$$+47.51e^{-16.5R_c} \times SNR - 1.36SNR \qquad \text{Equation 6.}$$

The $t_{optimal}$ on the left side of the equation represents the shortest incubation time required for accurate rate prediction. With modern optodes, the SNR is generally low enough to allow a very short incubation period according to Equation 6. The incubation length can be as short as 15 minutes, as shown by the "flat plane" area in Figure 9.

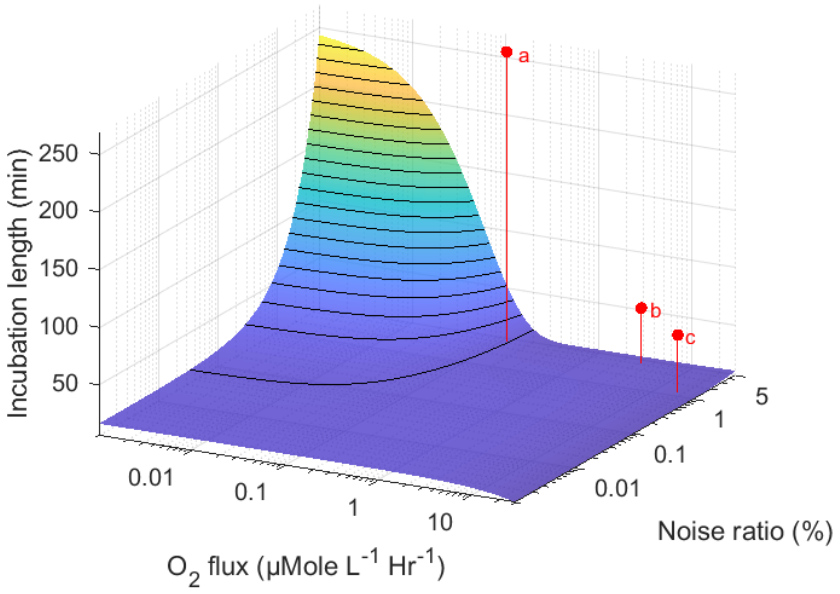

Figure 9. The surface represents the minimal incubation length needed to resolve targeted fluxes. The three red dots represent previous studies utilizing automated incubation techniques (Collins et al. 2019; Long et al. 2019). Point a, b, and c correspond to Collins' 2019 study in the North Atlantic basin, Long's 2019 study in Hog Reef, Bermuda, and Long's 2019 study in South Bay, Virginia, respectively.

Discussion

This study demonstrates the ability to quantify pelagic DO fluxes and their hourly variation in a shallow coastal ecosystem using an automated incubator. The DO optodes provide a high temporal resolution time series, enabling high-frequency (hourly) measurements of pelagic primary production and respiration. The high data density of the DO concentration time series allows the use of the Monte-Carlo simulation technique as opposed to the traditional calculation (e.g., two endpoints or linear regression). The Monte-Carlo simulation technique can resolve the dominant DO rates without the bias apparent in the linear regression models, especially when the time series does not resemble a straight-line shape. The hourly fluxes were useful for modeling the correlations between gross primary production (GPP) and available PAR, which was not possible with previous, lower-resolution techniques. The compilation of hourly flux rates also enabled

estimation of mean pelagic rates at the deployment site. Resolving these fluxes with higher temporal resolutions is essential for correctly assessing parameters of ecosystem metabolism such as NEM and GPP and determining the environmental drivers of these processes.

UV Treatment

UV treatment is the best candidate for a non-invasive, non-chemical approach for biofouling control. UV disinfection has been used for wastewater treatment and drinking water disinfection since the 1950s (Kruithof et al. 1992). Some UV wavelength is absorbed by nucleic acids in microorganisms, hindering the reproductive ability of targeted microorganisms to achieve inactivation (Gates, 1930). To mitigate the potential bias from biofouling in our deployments, the most effective UV dosage of 30 kJ m^{-2} was chosen. In this study, UV transparent plastic or quartz plates were installed over the light chamber to ensure sufficient UV dosage for the outside surface. Biofouling control outside of the chamber is especially important for light incubations. We observed no visible biofouling in or outside of the incubation chambers for both the UV transparent plastic covered chamber (with supplemental, external UV light) and the quartz covered chamber. The UV transparent plate needed external UV light because it only transmitted ~50% of UV irradiation while the quartz plate transmitted ~95% of UV irradiation. The UV dosage of our incubation system exceeds the EPA recommendations for UV disinfection by ~100 times for eliminating 99% of pathogens in drinking water (Schmelling, 2006), suggesting that a higher UV dosage may be required to maintain long-term biofouling control in marine applications. Such a high UV dosage relies on high power input, posing significant challenges for in-situ instrumentation. Recent studies have shown that given sufficient UV dosage, pulsing UV irradiation is more effective than continuous UV irradiation (Olsen et al. 2016; Zou et al. 2019). Pulsing UV irradiation also provides the technical advantage of driving UV LEDs with a higher

current to provide higher output, since LEDs can endure short periods of higher forward current. With pulsing UV irradiation, the irradiation duty cycles, and pulsing frequencies can be adjusted to minimize power consumption while maintaining high efficacy of biofouling control in future applications.

Non-linear Behavior in DO Timeseries

The Monte-Carlo simulation technique provided an important opportunity to improve timeseries analysis workflow. Segments of short DO time series data (e.g., 1 hour) often exhibited complicated behavior rather than an ideal straight line. The DO fluctuation represented not only the effects of photosynthesis and respiration but also the potential biases that contribute to the unsystematic behavior in the DO time series (Ducklow and Doney, 2013; Collins et al. 2018). Monte-Carlo simulation techniques were introduced to investigate the behavior of such complex systems (Harrison, 2009) and were employed here to reduce errors associated with simpler regression techniques. For example, a sharp decrease of DO concentration is occasionally observed from the dark chambers during daytime (Figure 10b). This is consistent with the observed "deep breath" phenomenon in a range of respiration research (Robert, 2012; Guillemette, McCallister, and del Giorgio, 2013). In the deep breath phenomenon, it is proposed that highly labile dissolved organic carbon (DOC) is rapidly respired during the initial phase of the incubation. The rate of respiration subsequently slows as the community shifts from the highly labile to semi-labile fractions of DOC. In other instances, the DO concentration showed net production for a portion of the incubation, then reverted to DO consumption after the initial production phase in the dark chamber. This observation can potentially be attributed to micro-bubble accumulation inside the chamber or on the optodes (Wikner et al. 2013; Collins et al. 2018).

While these examples could be ascribed to some other potential processes such as photorespiration, tidal influences, variability in temperature, variability in ambient light, mixing within the chamber, and inherent bottle effects, it is difficult to untangle the probable cause via hourly incubations (Bender et al. 1999; Jacquet et al. 2001; Robinson et al. 2002). Regardless, the Monte-Carlo simulation, as a probability simulation technique, does not depend on the shape of the entire time series to make predictions. As shown in Figure 10, Monte-Carlo simulation tends to generate rate estimates for the "predominant" trend in timeseries data— enabling quantification of the driving processes in timeseries data. The Monte-Carlo simulation technique is also important for developing a universal data analysis workflow since it requires minimal quality control for the raw data. This workflow is also essential in developing a protocol for autonomous incubation and operation (see Comments and Recommendations).

It is worth mentioning that the probability distribution of DO consumption/production rate can change depending on the random sampling function used (Harrison, 2009), and the number of repetitions set for simulation. In this study, a uniform probability distribution function is used to give equal probability in random sampling throughout the given incubation time series. The number of repetitions controls the density of the outcome histogram. The Monte-Carlo simulation tends to produce a "sharper" peak in the probability distribution spectrum with a significant proportion of calculated rates residing within the peak bin, while an insufficient number of repetitions often leads to a "flatter" probability distribution spectrum. An insufficient number of repetitions produces results more susceptible to the stochastic nature of random sampling. The convergence of simulation results with an increasing number of repetitions also suggests the linearity of respiration and photosynthesis rates under stable environmental conditions on an hourly timescale (del Giorgio and Williams, 2005).

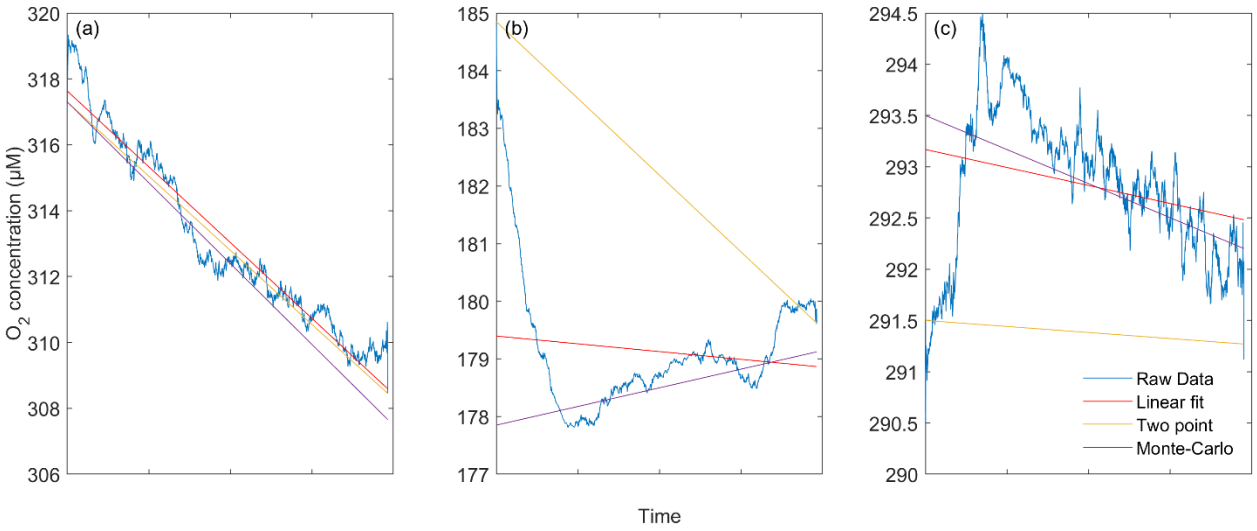

Figure 10. Comparison between different O_2 flux estimation methods. This figure sets show three different scenarios of raw data collected from field deployment on 8/26/2021-8/29/2021. Each subplot shows raw data and flux estimation from an incubation experiment (i.e., 50 minutes). 10(a) shows a simple respiration incubation, where the raw data evolves linearly, and all three flux estimation methods agree well with each other. 10(b) shows a sharp decrease of O_2 concentration and slow rebound. In this case, linear model failed to recognize either the downward or upward trend. 10(c) shows a sharp increase in O_2 concentration and then a steady drawdown. In this case, the two-point method failed to recognize any trend while the linear model was biased by the shape of the time series. Monte-Carlo simulation was affected by the sharp increase in O_2 concentration but produced results closer to predominant, steady decrease of O_2 concentration.

Comments and Recommendations

Automated sampling, high-frequency DO measurements, and new data analysis approaches have enabled this automated incubation system to sample and produce hourly DO fluxes. Resolving hourly fluxes is a significant improvement in temporal resolution compared to traditional in-situ and in-vitro methods. The recurring hourly sampling strategy also alleviates potential biases by providing many replicates through time. Data with high temporal resolution is also essential for resolving DO fluxes in dynamic environments such as coastal and estuarine ecosystems. In addition to applications in coastal and estuarine systems, the automated incubation system can also provide insight into sub-daily variation in the euphotic surface ocean, where metabolic rates remain largely unresolved due to the heterogeneity and complexity of biophysical interactions

(Ducklow and Doney, 2013). The hourly fluxes can also be integrated over time to produce the mean pelagic metabolic state. Integrating fluxes over time also provides better estimates of uncertainty/variability associated with metabolic fluxes in the open ocean (i.e., uncertainty in traditional methods is usually associated with analytical errors instead of variability in the natural environment). Automated hourly measurements can also provide more information for other acute environmental variations that influence metabolic activity in the water column as evidence suggests that metabolic rates change significantly on daily and hourly timescales (Caffrey, 2004; Staehr et al. 2012). There are numerous logistical advantages of automated incubation, including the acquisition of more data without the preparation of shipboard or laboratory incubations, and sampling in more inaccessible environments where acquiring and physically tending to samples is difficult.

The UV LEDs mitigate the previous concern of biofouling and the requirements of constant maintenance (Collins et al. 2018; Long et al. 2019). Biofouling control consumes the most power in this incubation system as an essential function. However, pulsing UV LEDs at shorter duty cycles and higher frequencies presents a promising solution to extend the deployment span and versatility of this instrument (Olsen et al. 2016; Zou et al. 2019). Future research on efficacy for integrated biofouling control with pulsing UV irradiation is needed to optimize instrument design and programming. A significantly reduced power demand also allows miniaturization in future designs while keeping the inherent bottle effects from small incubation volumes in mind. Future investigation into optimized surface-to-volume ratios for small-volume incubations is needed to guide the miniaturization of automated incubators. In an optimized design, a smaller incubation volume implies more efficiency in many engineering aspects (e.g., reducing pump/flush time, reducing UV irradiation output, reducing battery size). The miniaturization of a conceptualized

incubation system can unlock the potential for data collection on various platforms (e.g., floats, AUVs, moorings).

To achieve wider applicability, future designs should also take the length of incubation into account. For example, while the physical design of incubation volumes tends to be fixed based on the surface-to-volume ratio for biofouling and bottle effect control, incubation length can be programmed adaptively based on the initial observed rates to target the ideal incubation length to resolve fluxes. As a starting point for future studies, the Monte-Carlo simulation technique provides recommendations for incubation length based on targeted metabolic rates and sensor SNR (Figure 9). An adaptive sampling strategy could also be programmed as part of the algorithm in the microcontroller, adjusting incubation length during deployments based on the metabolic rates calculated from the raw DO time series. The adaptive sampling strategy will allow the optimization of the incubation experiment autonomously and in real-time, approaching the highest possible temporal resolution while maintaining data integrity.

In addition to improving the temporal resolution, this incubation technique also opens many opportunities for future developments. Specifically, improved spatial resolution can be achieved by deploying multiple units throughout the water column or in an array of horizontally spaced systems; the incoming light can be conditioned by using different chamber materials to investigate different processes (e.g., photosynthesis, respiration, photo-oxidation); and fluid sampling ports can be integrated for future collaboration with other in-situ sensors and lab-on-a-chip technology (Wang et al. 2015; Beaton et al. 2017; Vaughan et al. 2018). The ability to accommodate other in-situ sensors opens a wide range of applicability to incorporate many biogeochemical parameters (e.g., dissolved inorganic carbon, nitrate, phosphorus).

With the technological advantages discussed above, we believe this automated incubation technique provides many possibilities for advanced conceptual designs. A design of such conceptualized incubation systems should incorporate interdisciplinary efforts to assess the uncertainty of metabolic measurements, statistical approaches for data analysis, and engineering optimization. Consideration of design should include types of sensors used, materials used to construct the incubation chamber, shape and size of the incubation chamber, and wavelengths of UV irradiation used for efficient biofouling control— optimization of these elements would be essential to the success of future prototype development. We envision that an autonomous incubation system based on an adaptive sampling strategy and the Monte-Carlo simulation technique would greatly improve the understanding of pelagic metabolism and the longstanding discrepancies between methods to specifically address the lack of spatiotemporal resolution in pelagic metabolic rates.

Subsequent Development

Motivation

In continuance of the automated incubation system development, an updated version of automated incubation was developed to be an economical and easily scalable scientific instrument for autonomous operation. The previous prototypes (Collins et al. 2018, Long et al. 2019) tended to focus on resolving pelagic metabolic processes in a specific environment, with little flexibility for wider applications. For example, Long's early incubation system was designed for coastal and estuarine investigation; the system was simple, easy to deploy, and inexpensive (~$2k) but lacked the ability to resolve small DO rates and suffered from biofouling. Collins' incubation system was designed for open ocean application at greater depths but came with significant construction costs (~$75K) and biofouling concerns. Some of the vital issues across existing automated incubation

system design included (1) biofouling control with minimal labor or manual cleaning (2) modular design to allow measurements of different processes (e.g., photosynthesis, respiration) and (3) adaptability to different environments and platforms. Our previous, 3-chamber, incubation system was designed for coastal deployment as a standalone unit. The UV LED sterilized, multi-chamber design resolved concerns related to biofouling but aimed to resolve photosynthesis and respiration at the same time, resulting in a bulky package. The large incubation volume also required a substantial power supply for UV biofouling control to sustain longer deployments (i.e., a 26Ah battery can only support a ~72-hour deployment); it was heavy and required reassembly for maintenance and programming after deployment.

To address the issues mentioned above, the updated version of the automated incubation system was designed to be a miniaturized single-chamber system. The incubation volume was 50 ml, much smaller than the previous prototypes (e.g., 1L in the 3-chamber incubator, 250mL in Long's 2019 prototype, and 5.6 L in Collins' 2018 model). The smaller volume allowed lower UV irradiation dosage and the use of smaller pumps with lower overall power consumption. New low-power UV LEDs were used with pulse-width-modulation (PWM), which was reported to show better efficiency in biofouling control (Pedrós-Garrido et al. 2018, Fitzhenry et al. 2021). The system utilized an integrated quartz chamber to ensure full UV transmittance across the chamber walls. The incubation chamber was designed to sit on the top of the underwater housing and be easily replaced or reconfigured. The easily replaceable chamber provided flexibility to conduct different experiments with different chamber materials for light filtering (e.g., respiration in dark chambers, photosynthesis in light chambers, photo-oxidation in UV transparent chambers). The design also included a pressure-compensated pump housing to enable mesopelagic measurements, expanding the applicability of this new incubation system. This updated single-chamber incubation

system is designed to handle pressure/temperature changes and a longer deployment period. The overall package design was much smaller than the previous prototypes as well-- the integrated underwater housing is 2.5” Ø by 8.5” long, compared to 22” × 10” × 10” of the 3-chamber model. In addition to hardware updates, the system included software that corrects the optode DO output based on external temperature measurements. An integrated depth sensor was added to the design to enable autonomous deployment. The software also included functions to adjust incubation length based on the previously established relationships among targeted rates, sensor signal-to-noise ratio (SNR), and incubation time. We envisioned this single chamber incubation system to greatly expand the accessibility of measurements and data collection. The robust, autonomous, and miniaturized system design signified the first step towards adaptability with mobile vehicles, the deep sea, and remote deployments.

Material and Method

Hardware and Design

One of the most critical aspects of the new prototype development was modularization — each component of the incubation system could be easily replaced or serviced, even in the field. The main body of the incubation system contained an electronic housing for system operation and an incubation volume (Figure x). The electronic housing hosted an optode, an infrared (IR) temperature sensor, an ambient light sensor, an RGB neopixel, and UV LEDs. The incubation system is controlled by an advanced microcontroller (teensy 4.1, ARM Cortex-M7, 64-bit). A PyroScience optode (PICO-O2) was mounted behind the integrated quartz window for contactless sensing. The IR temperature sensor (MLX90614, Melexis Tech) was used to measure temperature in the incubation volume, the temperature was used for calibration and calculating DO concentration. The ambient light sensor (ALS-PT19-315C, Everlight Electronics) was used as an

auxiliary PAR measurement. The ambient light sensor was sensitive between 400-700 nm, which can be used for quality control for the dark chamber or providing additional PAR data for light chamber incubation. The RGB neopixel was used as a status indicator, showing different colors at various blinking rates for battery and experiment status (e.g., green blink for all system operational, red blink for low battery). There were 12 UV LEDs, separated into 3 strings of 4 LEDs on the UV LED array as a redundancy to ensure some level of UV irradiation even with malfunctioning LEDs. The UV LEDs were powered by a 12-24V boost buck (ABXS002A3_DS, GE) to provide sufficient forward voltage to each LED string. The LEDs strings were controlled with a transistor-MOSFET pair (2N3904, NTE, and IRFD9120, Vishay). The transistor-MOSFET pair allowed high-frequency PWM to regulate the UV dosage. The PWM by teensy 4.1 was programmed to pulse all UV LEDs with a 50% duty cycle at 256 Hz.

Above the electronic housing is the incubation volume. The incubation volume consisted of a base and an incubation chamber. The base of the incubation volume is mounted directly above the quartz window of the electronic housing. The base was designed to include spin and lock slots to hold the incubation chamber (Figure 12a). The base also hosted an integrated check valve as the sample inlet to the incubation volume, connected to the pump. The fluid path of the inlet is designed with an upward curve, intended to create a vortex within the chamber to facilitate the evacuation of microbubbles and particulates. As for the incubation chambers, there are currently 2 different materials used for incubation (1) a quartz chamber and (2) a 3D printed dark chamber. These chambers were designed to have a cylindrical shape with a conical top (Figure 12b). The conical top was designed to minimalize dead space for microbubbles. The upward fluid vortex and the conical top of the incubation volume should ensure optimal bubble evacuation.

In addition too the main body of the incubation, the system also included the pump and the battery housings. The pump housing and the battery housing could be mounted onto the main body of the incubation system separately or together with hose clamps. This design accommodated the potential uses for external pumps and alternative power sources. The 3D-printed housing hosted a diaphragm micropump (nf10TTPCB, KNF) with Tygon tubing and 3D-printed fluid paths. The pressure compensation compartment sat on top of the pump housing, including a 3D printed cap and custom-made rubber diaphragm (Bellophram). The pressure-compensated pump housing was filled with fluid (FC-40, 3M) to ensure minimal pressure difference. The battery housing was designed to host 9 D-cell batteries. We chose D-cell batteries to maximize adaptability. The incubation system would also accept any power options with 9-18V output.

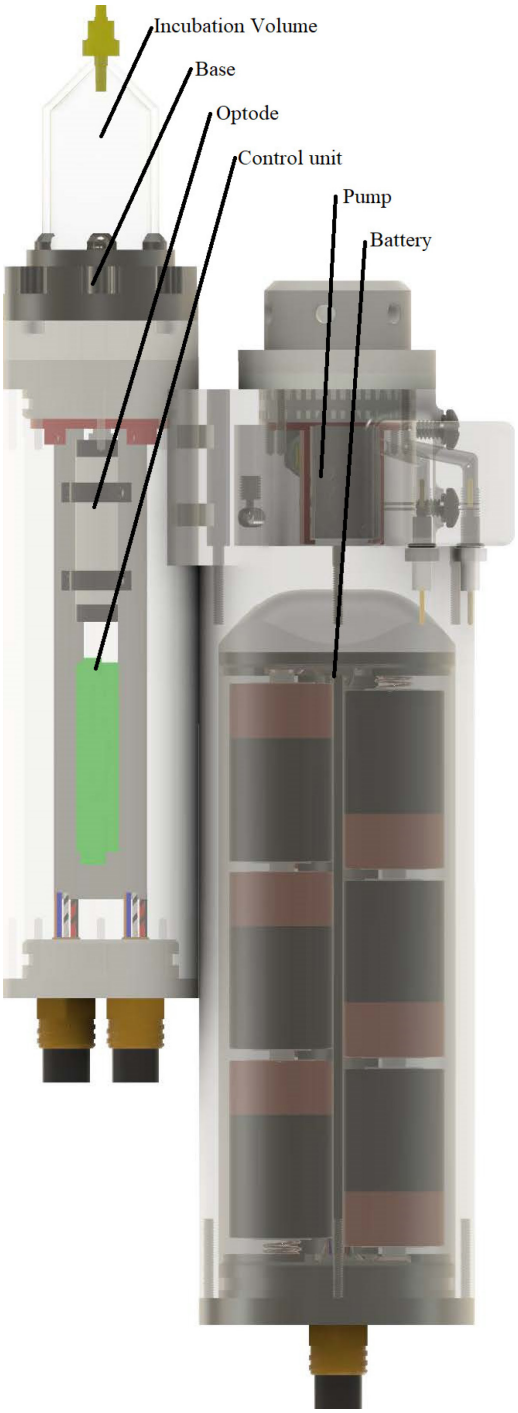

Figure 11. Overview of updated incubation system design. The incubation system was designed to consist of four major compartments: electronic housing, incubation volume, pump housing, and battery housing.

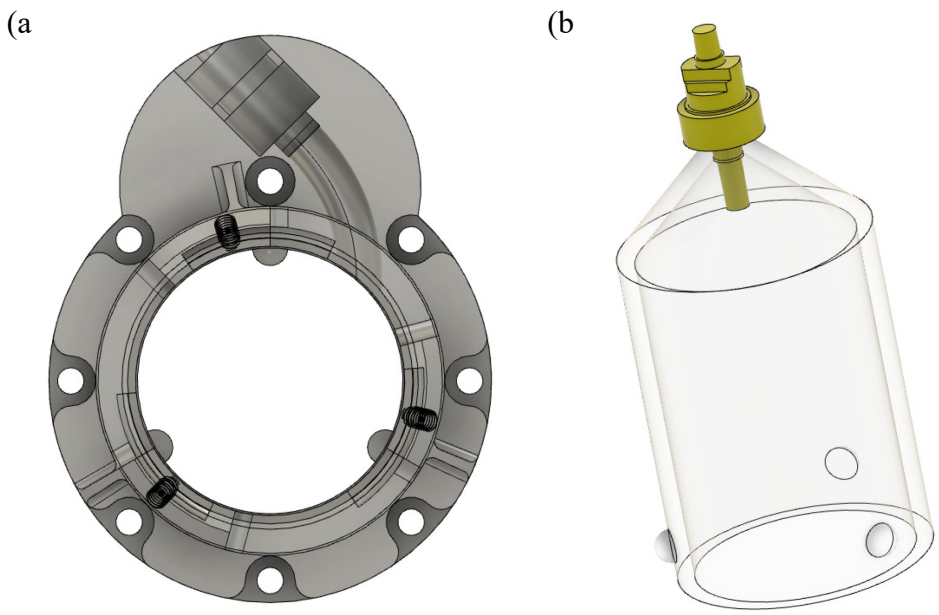

Figure 12. Overview of incubation volume design. (a) The base with upward spiral inlet to create fluid vortex in the incubation volume. The curve inlet on the top of the image shows the fluid path. (b) The conical top of the chamber and the check valve were designed to facilitate bubble evacuation during flushing.

Software and System Integration

In addition to hardware designs, this updated incubation system required many software features for autonomous operation and system integration. These new features included (1) pressure sensor calibration and feedback, (2) integrated optode calibration, and (3) adaptive sampling strategies. Firstly, the external pressure sensor allowed autonomous initialization of the instrument. The autonomous initialization is important for bubble evacuation and flushing the chamber with fresh samples at the beginning of the deployment. The external pressure sensor was programmed to calibrate itself at sea level and would initialize the incubation system once the depth reading had reached stability. Secondly, the integrated optode calibration was enabled by a custom calibration function that was adjustable based on a two-point calibration from the optode (i.e., the calibration took in degree phase shift reading from the optode at 0% and 100% DO for custom calibration

between degree phase shift and μMole). The custom calibration curve allowed the incubation to save raw data (degree phase shift) and then convert readings into the desired units. The raw data also provided more straightforward quality control and value correction with post-calibration. Thirdly, the adaptive sampling strategy used the relationship of optimal incubation length (Equation 6) to determine how long an incubation experiment should last. The targeted rate could either be set manually or the incubation system could estimate the rate from the first few incubation periods and then adjust the incubation length accordingly. Apart from the control of the incubation experiment, an integrated serial communication was included for software access without needing to open the underwater housing. Serial communication can handle data transfer, upload of operation codes, and on-the-fly control of the system. The data transfer protocol was written with a custom flow control protocol in Python. The main operation codes were written in Arduino environment and C++ codes. The custom calibration curve was written in MATLAB.

Summary

The updated automated incubation system seeks to combine engineering and research foci into a modular system and demonstrate their utility and capabilities. A pair of incubation system prototypes exist, have been tested in the lab, as well as in the coastal ocean, but not in the mesopelagic. (Notably, everything except the electronics housing was 3D printed, the circuit boards and drivers were fabricated and integrated in-house using rapid prototyping technology.) Software has been implemented to determine rates from Monte Carlo estimation and to automatically determine the required length for an experiment. CRITTR is also ready for serial communication with other platforms and systems. The central electronics housing is proven to be versatile and adaptable in the design and testing phase. Converting such modular incubation system for different experiment will involve simply snapping on a single module containing

incubation chamber of appropriate material, fluid handling apparatus, and accessory sensors. Modular components will allow an operator with an adapter to measure respiration in the deep-sea at pressure, photosynthesis at the surface by allowing light in through quartz chambers, in high- or low-fouling environments with variable UV anti-fouling, autonomously with its own integrated battery and buoyancy, as an epibiont on other vehicles or systems, or through communication with other systems or sensors that can trigger an experiment to begin based on external data or stimuli. These low-cost, small-scale, low-power incubation systems are oceanographic epibionts engineered to hitch a ride on a variety of existing moorings, gliders, floats, and AUVs. They will provide the next generation of autonomous C metabolic rates with inherently higher temporal resolution and radically higher spatial resolution. These small, economical incubation systems would enable a "fleet" of global rate measurements of photosynthesis and respiration throughout the ocean to inform global models and transform our understanding of oceanic carbon cycling.

Reference

Beaton, A. D., Wadham, J. L., Hawkings, J., Bagshaw, E. A., Lamarche-Gagnon, G., Mowlem, M. C., & Tranter, M. (2017). High-Resolution in Situ Measurement of Nitrate in Runoff

from the Greenland Ice Sheet. *Environmental Science and Technology*, *51*(21), 12518–12527. https://doi.org/10.1021/acs.est.7b03121

Bender, M., Orchardo, J., Dickson, M.-L., Barber, R., & Lindley, S. (1999). In vitro O2 fluxes compared with 14C production and other rate terms during the JGOFS Equatorial Pacific experiment. Deep Sea Research Part I: Oceanographic Research Papers, 46(4), 637–654. https://doi.org/https://doi.org/10.1016/S0967-0637(98)00080-6

Benway, H., Alin, S., Boyer, E., Cai, W.-J., Coble, P., Cross, J., Friedrichs, M., Goni, M., Griffith, P., Herrmann, M., Lohrenz, S., T. Mathis, J., Mckinley, G., G. Najjar, R., Pilskaln, C., Siedlecki, S., & Smith, R. (2016). *A Science Plan for Carbon Cycle Research in North American Coastal Waters*. https://doi.org/10.1575/1912/7777

Caffrey, J. (2004). *Factors Controlling Net Ecosystem Metabolism in U.S. Estuaries* (Vol. 27, Issue 1).

Collins, J. R., Fucile, P. D., McDonald, G., Ossolinski, J. E., Keil, R. G., Valdes, J. R., Doney, S. C., & van Mooy, B. A. S. (2018). An autonomous, in situ light-dark bottle device for determining community respiration and net community production. *Limnology and Oceanography: Methods*, *16*(6), 323–338. https://doi.org/10.1002/lom3.10247

del Giorgio, P. A., & Williams, P. J. (2005). *Respiration in Aquatic Ecosystems*. 1st ed. Oxford University Press.

Duarte, C. M., Regaudie-De-Gioux, A., Arrieta, J. M., Delgado-Huertas, A., & Agustí, S. (2013). The oligotrophic ocean is heterotrophic. *Annual Review of Marine Science*, *5*, 551–569. https://doi.org/10.1146/annurev-marine-121211-172337

Ducklow, H. W., & Doney, S. C. (2013). What is the metabolic state of the oligotrophic ocean? a debate. *Annual Review of Marine Science*, *5*, 525–533. https://doi.org/10.1146/annurev-marine-121211-172331

Fitzhenry, K., Clifford, E., Rowan, N. and del Rio, A.V., 2021. Bacterial inactivation, photoreactivation and dark repair post flow-through pulsed UV disinfection. Journal of Water Process Engineering, 41, p.102070.

G. Najjar, R., Herrmann, M., Alexander, R., Boyer, E., Burdige, D., Butman, D., Cai, W.-J., Canuel, E., Chen, B., Friedrichs, M., A. Feagin, R., Griffith, P. C., L. Hinson, A., Holmquist, J., Hu, X., M. Kemp, W., D. Kroeger, K., Mannino, A., Mccallister, S., & C. Zimmerman, R. (2018). Carbon Budget of Tidal Wetlands, Estuaries, and Shelf Waters of Eastern North America. *Global Biogeochemical Cycles*, *32*. https://doi.org/10.1002/2017GB005790

Gaarder, T., & Gran, H. H. (1927). Investigations of the production of plankton in the Oslo Fjord. *Rapports Et Proce`s-Verbaux Des Reunions Du Conseil Permanent International Pour L'Exploration*, *42*, 1–48.

Gates, F. L. (1930). A Study of the Bactericidal Action of Ultra Violet Light: III. The Absorption of Ultra Violet Light by Bacteria. *Journal of General Physiology*, *14*(1), 31–42. https://doi.org/10.1085/jgp.14.1.31

Goldman, J. A. L., Kranz, S. A., Young, J. N., Tortell, P. D., Stanley, R. H. R., Bender, M. L., & Morel, F. M. M. (2015). Gross and net production during the spring bloom along the Western Antarctic Peninsula. *New Phytologist*, *205*(1), 182–191. https://doi.org/10.1111/nph.13125

Guillemette, F., McCallister, S. L., & del Giorgio, P. A. (2013). Differentiating the degradation dynamics of algal and terrestrial carbon within complex natural dissolved organic carbon in temperate lakes. *Journal of Geophysical Research: Biogeosciences*, *118*(3), 963–973. https://doi.org/https://doi.org/10.1002/jgrg.20077

Hamme, R. C., & Emerson, S. R. (2006). Constraining bubble dynamics and mixing with dissolved gases: Implications for productivity measurements by oxygen mass balance. *Journal of Marine Research*, *64*(1), 73–95. https://doi.org/10.1357/002224006776412322

Harrison, R. L., Granja, C., & Leroy, C. (2010). Introduction to Monte Carlo Simulation. *Nuclear Physics Methods and Accelerators in Biology and Medicine.* 17–21. https://doi.org/10.1063/1.3295638

Jacquet, S., Partensky, F., Marie, D., Casotti, R., & Vaulot, D. (2001). Cell cycle regulation by light in prochlorococcus strains. Applied and Environmental Microbiology, 67(2), 782–790. https://doi.org/10.1128/AEM.67.2.782-790.2001

Kenner, R. A., & Ahmed, S. I. (1975). Measurements of electron transport activities in marine phytoplankton. *Marine Biology*, *33*(2), 119–127. https://doi.org/10.1007/BF00390716

Kruithof, J., Leer, R., & Hijnen, W. (1992). Practical Experiences with UV-Disinfection in the Netherlands. *J. Water SRT - Aqua*, *41*, 88–94.

Lee, J. S., An, S.-U., Park, Y.-G., Kim, E., Kim, D., Kwon, J. N., Kang, D.-J., & Noh, J.-H. (2015). Rates of total oxygen uptake of sediments and benthic nutrient fluxes measured using an in situ autonomous benthic chamber in the sediment of the slope off the southwestern part of Ulleung Basin, East Sea. *Ocean Science Journal*, *50*(3), 581–588. https://doi.org/10.1007/s12601-015-0053-x

Long, M. H., Rheuban, J. E., McCorkle, D. C., Burdige, D. J., & Zimmerman, R. C. (2019). Closing the oxygen mass balance in shallow coastal ecosystems. *Limnology and Oceanography*, *0*(0). https://doi.org/10.1002/lno.11248

Moore, C., Barnard, A., Fietzek, P., Lewis, M. R., Sosik, H. M., White, S., & Zielinski, O. (2009). Optical tools for ocean monitoring and research. In *Ocean Sci* (Vol. 5). www.ocean-sci.net/5/661/2009/

Nelson, T. F., Reddy, C. M., & Ward, C. P. (2021). Product Formulation Controls the Impact of Biofouling on Consumer Plastic Photochemical Fate in the Ocean. *Environmental Science and Technology*, *55*(13), 8898–8907. https://doi.org/10.1021/acs.est.1c02079

Nielsen, E. S. (1952). The Use of Radio-active Carbon (C14) for Measuring Organic Production in the Sea. *ICES Journal of Marine Science*, *18*(2), 117–140. https://doi.org/10.1093/icesjms/18.2.117

Olsen, R. O., Hoffmann, F., Hess-Erga, O. K., Larsen, A., Thuestad, G., & Hoell, I. A. (2016). Ultraviolet radiation as a ballast water treatment strategy: Inactivation of phytoplankton measured with flow cytometry. *Marine Pollution Bulletin*, *103*(1–2), 270–275. https://doi.org/10.1016/j.marpolbul.2015.12.008

Pedrós-Garrido, S., Condón-Abanto, S., Clemente, I., Beltrán, J.A., Lyng, J.G., Bolton, D., Brunton, N. and Whyte, P., 2018. Efficacy of ultraviolet light (UV-C) and pulsed light (PL) for the microbiological decontamination of raw salmon (Salmo salar) and food contact surface materials. *Innovative Food Science & Emerging Technologies*, *50*, pp.124-131.

Palevsky, H. I., & Doney, S. C. (2018). How Choice of Depth Horizon Influences the Estimated Spatial Patterns and Global Magnitude of Ocean Carbon Export Flux. Geophysical Research Letters, 45(9), 4171–4179. https://doi.org/https://doi.org/10.1029/2017GL076498

Quay, P. D., Peacock, C., Bjrkman, K., & Karl, D. M. (2010). Measuring primary production rates in the ocean: Enigmatic results between incubation and non-incubation methods at Station ALOHA. *Global Biogeochemical Cycles*, *24*(3). https://doi.org/10.1029/2009GB003665

Reinthaler, T., van Aken, H. M., & Herndl, G. J. (2010). Major contribution of autotrophy to microbial carbon cycling in the deep North Atlantic's interior. *Deep-Sea Research Part II: Topical Studies in Oceanography*, *57*(16), 1572–1580. https://doi.org/10.1016/j.dsr2.2010.02.023Robert, A. 2012.

Robinson, C., Serret, P., Tilstone, G., Teira, E., Zubkov, M. v, Rees, A. P., & Woodward, E. M. S. (2002). Plankton respiration in the Eastern Atlantic Ocean. Deep Sea Research Part I: Oceanographic Research Papers, 49(5), 787–813. https://doi.org/https://doi.org/10.1016/S0967-0637(01)00083-8

Mineralisation in situ de la matie`re organique le long de la colonne d'eau: Application surune station eulerienne. Dissertation. Universite d'Aix-Marseille.

Schmelling, D. (2006). Ultraviolet Disinfection Guidance Manual for the Final Long TermEnhanced Surface Water Treatment Rule. EPA. http://www.epa.gov/safewater/disinfection/lt2/compliance.html

Spanjers, H., Olsson, G., & Klapw1jk, A. (1994). Determining Short-Term Biochemical Oxygen Demand and Respiration Rate in an Aeration Tank by Using Respirometry and Estimation. In *War. Res* (Vol. 28, Issue 93).

Staehr, P. A., Testa, J. M., Kemp, W. M., Cole, J. J., Sand-Jensen, K., & Smith, S. v. (2012). The metabolism of aquatic ecosystems: History, applications, and future challenges. In *Aquatic Sciences* (Vol. 74, Issue 1, pp. 15–29). https://doi.org/10.1007/s00027-011-0199-2

Suter, E. A., Scranton, M. I., Chow, S., Stinton, D., Medina Faull, L., & Taylor, G. T. (2017). Niskin bottle sample collection aliases microbial community composition and biogeochemical interpretation. *Limnology and Oceanography*, *62*(2), 606–617. https://doi.org/10.1002/lno.10447

Vaughan, M. C. H., Bowden, W. B., Shanley, J. B., Vermilyea, A., Wemple, B., & Schroth, A. W. (2018). Using in situ UV-Visible spectrophotometer sensors to quantify riverine phosphorus partitioning and concentration at a high frequency. *Limnology and Oceanography: Methods*, *16*(12), 840–855. https://doi.org/10.1002/lom3.10287

Wang, Z. A., Sonnichsen, F. N., Bradley, A. M., Hoering, K. A., Lanagan, T. M., Chu, S. N., Hammar, T. R., & Camilli, R. (2015). In situ sensor technology for simultaneous spectrophotometric measurements of seawater total dissolved inorganic carbon and pH. *Environmental Science and Technology*, *49*(7), 4441–4449. https://doi.org/10.1021/es504893n

Ward, C. (2021). A Bright, LED-Lit Future for Ocean Sciences. *Eos*, *102*. https://doi.org/10.1029/2021EO210674

Wikner, J., Panigrahi, S., Nydahl, A., Lundberg, E., Båmstedt, U., & Tengberg, A. (2013). Precise continuous measurements of pelagic respiration in coastal waters with Oxygen Optodes. *Limnology and Oceanography: Methods*, *11*(JAN), 1–15. https://doi.org/10.4319/lom.2013.11.1

Williams, P. J. L. B., Morris, P. J., & Karl, D. M. (2004). Net community production and metabolic balance at the oligotrophic ocean site, station ALOHA. *Deep-Sea Research Part I: Oceanographic Research Papers*, *51*(11), 1563–1578. https://doi.org/10.1016/j.dsr.2004.07.001

Williams, P. J. L. B., Quay, P. D., Westberry, T. K., & Behrenfeld, M. J. (2013). The oligotrophic ocean is autotrophic. *Annual Review of Marine Science*, *5*, 535–549. https://doi.org/10.1146/annurev-marine-121211-172335

Zou, X. Y., Lin, Y. L., Xu, B., Cao, T. C., Tang, Y. L., Pan, Y., Gao, Z. C., & Gao, N. Y. (2019). Enhanced inactivation of E. coli by pulsed UV-LED irradiation during water disinfection. *Science of the Total Environment*, *650*, 210–215.https://doi.org/10.1016/j.scitotenv.2018.08.367